

# Transcriptome-based profiling of yolk sac-derived macrophages reveals a role for *Irf8* in macrophage maturation

Nora Hagemeyer<sup>1,†</sup>, Katrin Kierdorf<sup>1,†</sup>, Kathrin Frenzel<sup>1,†</sup>, Jia Xue<sup>2</sup>, Marc Ringelhan<sup>3,4</sup>, Zeinab Abdullah<sup>5</sup>, Isabelle Godin<sup>6</sup>, Peter Wieghofer<sup>1</sup>, Marta Joana Costa Jordão<sup>1</sup>, Thomas Ulas<sup>2</sup>, Gülden Yorgancioglu<sup>1</sup>, Frank Rosenbauer<sup>7</sup>, Percy A Knolle<sup>8</sup>, Mathias Heikenwalder<sup>3,9</sup>, Joachim L Schultze<sup>2,10</sup> & Marco Prinz<sup>1,11,\*</sup>

## Abstract

Recent studies have shown that tissue macrophages (MΦ) arise from embryonic progenitors of the yolk sac (YS) and fetal liver and colonize tissues before birth. Further studies have proposed that developmentally distinct tissue MΦ can be identified based on the differential expression of F4/80 and CD11b, but whether a characteristic transcriptional profile exists is largely unknown. Here, we took advantage of an inducible fate-mapping system that facilitated the identification of CD45<sup>+</sup>c-kit<sup>-</sup>CX<sub>3</sub>CR1<sup>+</sup>F4/80<sup>+</sup> (A2) progenitors of the YS as the source of F4/80<sup>hi</sup> but not CD11b<sup>hi</sup> MΦ. Large-scale transcriptional profiling of MΦ precursors from the YS stage to adulthood allowed for building computational models for F4/80<sup>hi</sup> tissue macrophages being direct descendants of A2 progenitors. We further identified a distinct molecular signature of F4/80<sup>hi</sup> and CD11b<sup>hi</sup> MΦ and found that *Irf8* was vital for MΦ maturation. Our data provide new cellular and molecular insights into the origin and developmental pathways of tissue MΦ.

**Keywords** CX3CR1; fate mapping; gene profiling; Kupffer cells; macrophages; microglia

**Subject Categories** Immunology

**DOI** 10.15252/embj.201693801 | Received 4 January 2016 | Revised 13 June 2016 | Accepted 15 June 2016 | Published online 13 July 2016

**The EMBO Journal (2016) 35: 1730–1744**

## Introduction

Macrophages (MΦ) play an important role in maintaining tissue integrity and contribute to adaptive and innate immune responses. They are part of the mononuclear phagocyte system and were classically thought to derive from blood monocytes (van Furth & Cohn, 1968). This concept prevailed for nearly half a century (Ginhoux & Jung, 2014). Accumulating evidence, however, including recent studies using sophisticated fate-mapping approaches, has determined that some tissue MΦ and their precursors are established embryonically in the yolk sac (YS) and fetal liver before the onset of hematopoiesis in the bone marrow (Ginhoux *et al*, 2010; Hoeffel *et al*, 2012; Schulz *et al*, 2012; Epelman *et al*, 2014; Molawi *et al*, 2014; Gomez *et al*, 2015). However, conflicting reports have recently been published suggesting a different origin for all tissue macrophages except microglia from sources of the definitive hematopoiesis (Sheng *et al*, 2015). Thus, the origin of tissue macrophages still awaits its full discovery. We therefore adapted our recently established *Cx3cr1<sup>CreER</sup>* fate-mapping system (Goldmann *et al*, 2013; Yona *et al*, 2013) to unequivocally determine the temporal and spatial origin of tissue macrophages and to investigate their full transcriptional program during ontogeny from the YS until adulthood.

Regardless of their origin, tissue MΦ can maintain themselves in adulthood through self-renewal and thus independently of blood monocytes (Ajami *et al*, 2007; Mildner *et al*, 2007; Hashimoto *et al*, 2013; Sieweke & Allen, 2013; Yona *et al*, 2013). Recent studies have further proposed that the expression levels of the markers F4/80 and CD11b can be used to identify ontogenetically distinct MΦ

- 1 Institute of Neuropathology, University of Freiburg, Freiburg, Germany
- 2 Genomics and Immunoregulation, LIMES-Institute, University of Bonn, Bonn, Germany
- 3 Institute of Virology, Technische Universität München/Helmholtz-Zentrum Munich, Munich, Germany
- 4 Second Medical Department, Klinikum rechts der Isar, Technische Universität München, Munich, Germany
- 5 Institute of Experimental Immunology, University Bonn, Bonn, Germany
- 6 Gustave Roussy, INSERM U1170, Université Paris-Saclay, Villejuif, France
- 7 Institute of Molecular Tumor Biology, University of Muenster, Muenster, Germany
- 8 Institute of Molecular Immunology, Technische Universität München, Munich, Germany
- 9 Division of Chronic Inflammation and Cancer, German Cancer Research Center (DKFZ), Heidelberg, Germany
- 10 Platform for Single Cell Genomics and Epigenomics, German Center for Neurodegenerative Diseases, University of Bonn, Bonn, Germany
- 11 BIOSS Centre for Biological Signalling Studies, University of Freiburg, Freiburg, Germany

\*Corresponding author. Tel: +49 761 270 51050; Fax: +49 761 270 50500; E-mail: marco.prinz@uniklinik-freiburg.de

†These authors contributed equally to this work

populations in various tissues, but failed to determine genetic traits underlying this supposed heterogeneity (Schulz *et al*, 2012; Bain *et al*, 2014). Previous gene expression profiling of M $\Phi$  populations from several tissues has established that only a small number of mRNA transcripts were associated with all M $\Phi$  but not DCs. However, a core gene signature of all macrophages could be detected (Gautier *et al*, 2012). The impact of the tissue environment on M $\Phi$  signatures is now beginning to be unraveled. Epigenetic modifications are one of the conduits through which the organ-specific environment can influence the established M $\Phi$  identities. The chromatin landscape, among other epigenomic features of a differentiated cell type, reflects both its developmental origin as well as its future potential. Two recent studies compared the tissue M $\Phi$  enhancer repertoire that revealed a tissue-specific signature with considerable plasticity (Gosselin *et al*, 2014; Lavin *et al*, 2014).

However, the regulatory networks, the precise ancestry, and the mechanisms that describe tissue M $\Phi$  development from the YS stage to adulthood are largely unknown. By combining large-scale transcriptome profiling with fate mapping, immunophenotyping, and confocal imaging, we provide a detailed description of F4/80<sup>hi</sup> tissue M $\Phi$  development from uncommitted erythromyeloid precursors (EMP; CD45<sup>+</sup>c-kit<sup>+</sup>) via the M $\Phi$  ancestor populations A1 (CD45<sup>+</sup>c-kit<sup>lo</sup>CX<sub>3</sub>CR1<sup>lo</sup>F4/80<sup>lo</sup>) and A2 (CD45<sup>+</sup>c-kit<sup>-</sup>CX<sub>3</sub>CR1<sup>+</sup>F4/80<sup>+</sup>) in the YS to embryonic M $\Phi$  and then fully differentiated M $\Phi$  during adulthood. By using an A2 cell type-based fate-mapping system that tracks distinct YS cells, we can furthermore show that in contrast to a recent report (Sheng *et al*, 2015) several tissues contain F4/80<sup>hi</sup> M $\Phi$  that are derived from the YS. Moreover, besides anticipated tissue environment-related genetic differences, we could identify a core signature in the embryonic and adult F4/80<sup>hi</sup> and CD11b<sup>hi</sup> M $\Phi$  population.

We further identified a transcriptional factor that is essential for both F4/80<sup>hi</sup> and CD11b<sup>hi</sup> M $\Phi$  homeostasis *in vivo*. There are several transcription factors proven to be important for myeloid cell development including Pu.1, which affects multiple lineages of the hematopoiesis in an early stage including the development of M $\Phi$  (Rosenbauer & Tenen, 2007). Additional transcription factors have been reported to play a role in the differentiation of myeloid cells such as *interferon regulatory factor 8* (*Irf8*) as a transcriptional factor of the IRF family (Rosenbauer & Tenen, 2007). IRF-8 interacts with other transcription factors such as IRF-1, IRF-2, IRF-4 and PU.1 (Tamura & Ozato, 2002). It is known that *Irf8* has critical roles in the differentiation of myeloid cells, promoting monocyte over granulocyte differentiation (Tamura & Ozato, 2002). It is also a crucial regulator of many aspects of DC development, differentiation, and function (Tamura *et al*, 2008), thus holding an essential role in the establishment of innate immune responses. Although *Irf8* is critical for the regulation of several myeloid cell lineages derived from hematopoietic stem cells (HSCs) including bone marrow-derived macrophages (Tamura & Ozato, 2002), its role for tissue macrophages emerged from prenatal precursors from the YS or fetal liver, independent from HSCs, is unclear. In fact, recent work proposed a vital role of IRF-8 only for circulating monocytes but not for tissue macrophages (Hambleton *et al*, 2011). In contrast to that report we show that both M $\Phi$  subsets (F4/80<sup>hi</sup> and CD11b<sup>hi</sup>) are strongly dependent on the transcription factor *Irf8*, which in our study influenced M $\Phi$  homeostasis. Our findings substantially increase the understanding of the regulatory processes that characterize tissue

M $\Phi$  development in a highly dynamic microenvironment from the YS stage until adulthood.

## Results

### Temporospatial *in vivo* fate mapping and transcriptomics defines F4/80<sup>hi</sup> M $\Phi$ as descendants of A2 progenitors

In mice, the first hematopoietic progenitors appear in the extra-embryonic YS where they generate nucleated erythrocytes and M $\Phi$  starting at embryonic day (E) 7.5–8.0 (Bertrand *et al*, 2005; Cumano & Godin, 2007). From E 8.0, multilineage erythromyeloid progenitors (EMPs) emerge in the YS as a second wave that are thought to give rise to tissue M $\Phi$  in the brain (Kierdorf *et al*, 2013; Prinz & Priller, 2014) and other tissues as well (Gomez *et al*, 2015). After E 9.0, the intra-embryonic mesoderm commits to the hematopoietic lineage and new waves of hematopoietic progenitors emerge: first in the para-aortic splanchnopleura (P-Sp) region and then in the aorta-gonad-mesonephros (AGM) region (Cumano & Godin, 2007).

To follow the fate of myeloid cells during early embryogenesis, we first used *Cx3cr1*<sup>GFP/WT</sup> mice, which have a GFP knock-in on one allele of the *Cx3cr1* gene. CX<sub>3</sub>CR1 is expressed in mature monocytes as well as many tissue M $\Phi$  and their precursors (Yona *et al*, 2013). To determine at which time point the YS contains progenitor cells with M $\Phi$  features, we analyzed E 9.0 embryos by thorough confocal microscopy (Fig 1A and B). We detected two distinct populations in the YS at this time point: CD31<sup>+</sup>c-kit<sup>+</sup> EMPs and CX<sub>3</sub>CR1<sup>+</sup>F4/80<sup>+</sup> early M $\Phi$  (Bertrand *et al*, 2005). Notably, CX<sub>3</sub>CR1<sup>+</sup>F4/80<sup>+</sup> cells were found in the YS but not in the P-Sp region indicating a largely YS-centered localization of early M $\Phi$  progenitors at this developmental stage. By separation of CD45<sup>+</sup> cells, we were able to discriminate between two M $\Phi$  precursor subsets, CD45<sup>+</sup>CX<sub>3</sub>CR1<sup>lo</sup>F4/80<sup>lo</sup> A1 cells and CD45<sup>+</sup>CX<sub>3</sub>CR1<sup>hi</sup>F4/80<sup>hi</sup> A2 progenitors as described before (Bertrand *et al*, 2005; Kierdorf *et al*, 2013) (Fig 1C).

From our previous studies, we know that microglia derive from the A2 progenitors of the YS (Kierdorf *et al*, 2013). Recently, it was suggested that the progenitor for microglia and other tissue M $\Phi$  are different from each other (Hoeffel *et al*, 2015; Sheng *et al*, 2015). However, our hypothesis was that F4/80<sup>hi</sup> M $\Phi$  derive from the A2 progenitors of the YS as well. To perform fate mapping and subsequent gene profiling of tissue M $\Phi$  during ontogeny, we next adapted our recently developed *Cx3cr1*<sup>CreER</sup> mouse system (Goldmann *et al*, 2013; Yona *et al*, 2013) to target A2 progenitors only (Fig 1D). Male *Cx3cr1*<sup>CreER</sup>: *Rosa26-fl-STOP-fl-yfp* (*Cx3cr1*<sup>CreER</sup>:*Rosa26-yfp*) mice were crossed to female wild-type mice, and plug-positive animals were injected with a single intraperitoneal dose of tamoxifen (TAM) at E 9.0. The application of TAM at E 9.0 induced the recombination of CX<sub>3</sub>CR1<sup>+</sup> progenitor cells and therefore also targeted A2-derived microglia (Fig EV1A and B). Importantly, to prove the specificity of our approach, we additionally investigated the recombination efficiency in microglia of E 16.0 embryos after TAM application at E 7.0 and E 8.0 (Fig EV1B). TAM application at E 8.0 but not at E 7.0 was able to target a small population of A2-derived microglia (YFP<sup>+</sup> cells = 17.7 ± 1.3%) as well as liver (YFP<sup>+</sup> cells = 13.2 ± 1.4%) and kidney (YFP<sup>+</sup> cells = 15 ± 3.1%) F4/80<sup>hi</sup> M $\Phi$ . This result shows that the TAM-induced Cre recombination is restricted to a very limited time window of maximal 1 day. No CX<sub>3</sub>CR1<sup>+</sup> HSCs

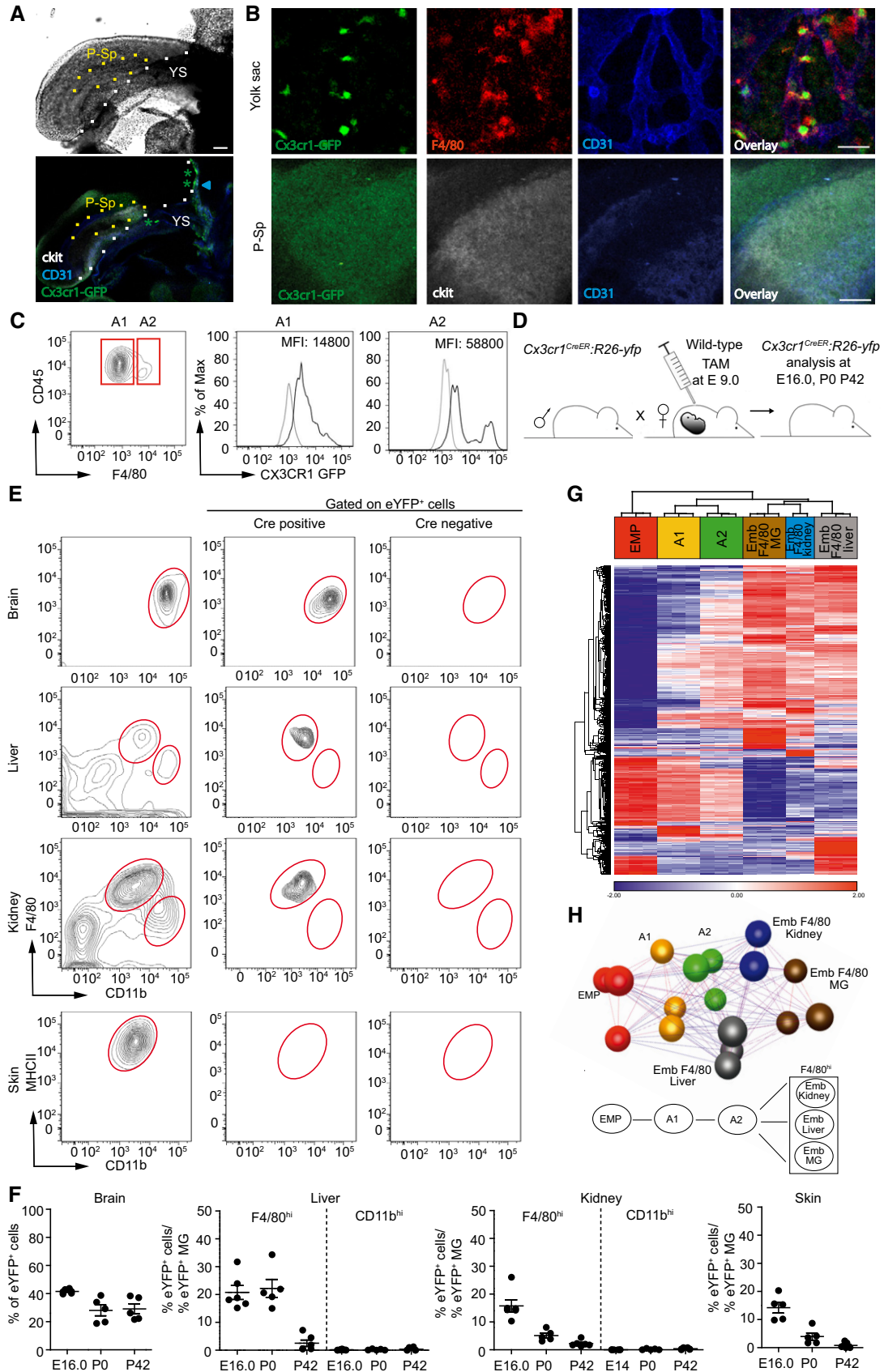


Figure 1.

**Figure 1. Temporospatial *in vivo* fate mapping of yolk sac MΦ and transcriptional ancestry of F4/80<sup>hi</sup> tissue MΦ during ontogeny.**

- A Overview images of hematopoietic sites in an E 9.0 embryo depicting the yolk sac (YS) and para-aortic splanchnopleura region (P-Sp) with phase contrast (upper image) and direct fluorescence microscopy (lower image). Stars indicate CX<sub>3</sub>CR1<sup>+</sup> cells (green) and arrowhead points to c-kit<sup>+</sup>/CD31<sup>+</sup> EMPs (blue/white) in the YS. Scale bar represents 100 μm. One representative picture out of five independent experiments is displayed.
- B Higher magnifications of the YS and P-Sp. CX<sub>3</sub>CR1-GFP expression (green) is found in the YS but not in the P-Sp, where only background staining is present. F4/80 (red), CD31 (blue), c-kit (white). Scale bars represent 50 μm. Representative pictures out of five independent experiments are shown.
- C Flow cytometric analysis of MΦ precursors in the YS of E 9.0 *Cx3cr1<sup>GFP/WT</sup>* animals (A1: CD45<sup>+</sup>c-kit<sup>lo</sup>CX<sub>3</sub>CR1<sup>lo</sup>F4/80<sup>lo</sup>, A2: CD45<sup>+</sup>c-kit<sup>-</sup>CX<sub>3</sub>CR1<sup>+</sup>F4/80<sup>+</sup>). Mean fluorescent intensity (MFI) is presented. Four mice were investigated showing similar results.
- D Fate-mapping strategy to target the A2 progenitor population preferentially in the YS. Male *Cx3cr1<sup>CreER</sup>;R26-yfp* mice were bred to wild-type animals, and plug-positive mice were injected at E 9.0 with tamoxifen (TAM). Offspring was analyzed at E 16.0, P0 or P42.
- E Flow cytometry of F4/80<sup>hi</sup>CD11b<sup>lo</sup> and F4/80<sup>lo</sup>CD11b<sup>hi</sup> tissue MΦ in adult (P42) *Cx3cr1<sup>CreER</sup>;R26-yfp* mice. Cre-negative mice served as a control. Representative histograms from three independent experiments are displayed.
- F Quantification of YFP labeling in tissue MΦ at E 16.0, P0, and P42 after TAM application at E 9.0 in plug-positive *Cx3cr1<sup>CreER</sup>;R26-yfp* mice. Data are normalized to YFP<sup>+</sup> microglia and presented as mean ± s.e.m. At least one experiment out of two is shown, and each symbol presents one mouse.
- G Hierarchical clustering of the 1,000 most variable probes within the dataset of embryonic development of yolk sac-derived tissue MΦ (EMP: erythromyeloid precursor, A1/A2: yolk sac MΦ progenitors, Emb F4/80 MG: embryonic microglia, Emb F4/80 liver: embryonic Kupffer cells, Emb F4/80 kidney: embryonic F4/80 kidney cells). Heat map displays z-transformed log<sub>2</sub>-expression values from red to blue via white.
- H Above: Sample-wise co-regulation network of embryonic MΦ development. Pearson correlation threshold of 0.92 was used to generate the network. Below: scheme thereof.

were present in the E 10.0/E 10.5 AGM or fetal liver proving that we do not target HSCs in our approach (Fig EV1C and D). Therefore, specific targeting of A2 progenitors by TAM injection at E 9.0 induced efficient YFP labeling of 41.6 ± 0.6% brain microglia, 20.8 ± 2.5% F4/80<sup>hi</sup> Kupffer cells, 15.8 ± 2.2% F4/80<sup>hi</sup> kidney MΦ, and 14.2 ± 1.9% MHC II<sup>+</sup> CD11b<sup>+</sup> skin MΦ at E 16.0, indicating robust labeling efficiency of various A2-derived MΦ progeny (Fig 1F). Microglia in 6-week-old animals retained the YFP label, demonstrating that A2-derived cells persists until adulthood, whereas labeling of Kupffer cells, Langerhans cells, and F4/80<sup>hi</sup> kidney cells was present but dropped after birth (Figs 1E and F, EV1E and EV2). This might be due to a replacement by fetal liver-derived cells as suggested by others (Hoeffel *et al*, 2012; Gomez *et al*, 2015). In contrast, CD11b<sup>hi</sup> tissue MΦ were not labeled in this approach (Fig 1E and F). Collectively, these data suggest that F4/80<sup>hi</sup> tissue MΦ are initially derived from CX<sub>3</sub>CR1<sup>+</sup> A2 cells in the YS, whereas CD11b<sup>hi</sup> tissue MΦ develop independently from A2 cells.

After having established an A2 YS-dependent labeling system, we isolated EMP from E 8.0 YS, A1 and A2 cells from E 9.0 YS, and embryonic F4/80<sup>hi</sup> MΦ from E 14.5 brain, liver, and kidney and performed a whole-genome expression analysis using the Affymetrix Mouse Gene 2.1 ST Array. Subsequent investigation of the 1,000 most variable transcripts by hierarchical clustering (Fig 1G) and generating a co-regulation network based on all expressed transcripts (Fig 1H) revealed that EMPs represent an early step in MΦ hierarchy followed by the YS populations A1 and A2, while A2 cells obviously represent a nodal point of tissue MΦ development (Fig 1G and H). These data suggest that the MΦ populations analyzed gain their own tissue-specific signature once they have left the YS and that A2 YS progenitors are ancestors of embryonic F4/80<sup>hi</sup> tissue MΦ.

**Difference in maintenance of F4/80<sup>hi</sup> and CD11b<sup>hi</sup> MΦ after birth**

Once established in the CNS, microglia persist throughout the entire life of the organism without any significant input from circulating blood cells due to their longevity and their capacity for self-renewal (Ajami *et al*, 2007; Mildner *et al*, 2007). We therefore sought to use this unique feature of microglia to compare the kinetics of persistence with F4/80<sup>hi</sup> and CD11b<sup>hi</sup> cells from the kidney and liver. For this purpose, we induced adult *Cx3cr1<sup>CreER</sup>;R26-yfp* animals with

TAM and determined MΦ labeling at several time points after application (Fig 2A–C). FACS analysis demonstrated long-term labeling of microglia and F4/80<sup>hi</sup> kidney MΦ with virtually no turnover in microglia and low turnover in F4/80<sup>hi</sup> kidney MΦ (exchange rate: approx. 2%/week). In contrast, YFP labeling rapidly dropped in CD11b<sup>hi</sup> cells in liver and kidney indicating higher turnover rates (approx. 32%/week for both organs). Notably, Kupffer cells dynamically express CX<sub>3</sub>CR1 during development but lose their expression shortly after birth which is why their turnover cannot be monitored during adulthood (Yona *et al*, 2013). To circumvent these limitations, we adapted our *Cx3cr1<sup>CreER</sup>;R26-yfp* system and induced recombination shortly after birth when F4/80<sup>hi</sup> Kupffer cells still express CX<sub>3</sub>CR1 (Fig 2C). We successfully targeted at least a subpopulation of the F4/80<sup>hi</sup> Kupffer cells. Similar to their relatives in the brain, this Kupffer cell population remained a remarkably stable population until 9 months of age. To evaluate a possible contribution of blood cells to the macrophage populations, we evaluated the contribution of both Ly6C<sup>hi</sup> and Ly6C<sup>lo</sup> monocytes. We first measured the expression of monocyte-related CCR2 that was absent on F4/80<sup>hi</sup> Kupffer cells, only partially present on F4/80<sup>hi</sup> kidney MΦ but clearly present on CD11b<sup>hi</sup> MΦ (Fig 2D). Furthermore, we provide genetic evidence that Ly6C<sup>hi</sup> monocytes contributed to the homeostasis of F4/80<sup>hi</sup> kidney MΦ as well as CD11b<sup>hi</sup> MΦ shown by reduced cell numbers in mice lacking *Ccr2* (Fig 2E). In contrast, Ly6C<sup>lo</sup> monocytes were dispensable for F4/80<sup>hi</sup> and CD11b<sup>hi</sup> MΦ development and homeostasis as mice lacking *Nr4a1* presented with normal amounts of MΦ subsets in liver and kidney (Fig 2E). These data indicate that adult microglia and Kupffer cells are stable populations which do not undergo significant exchange with blood cells within the first 9 months of life. In contrast, adult F4/80<sup>hi</sup> kidney MΦ are partially replaced by blood monocytes, whereas adult CD11b<sup>hi</sup> MΦ found in the liver and kidney have a fast and continuous exchange with circulating CCR2-dependent progenitors, most likely Ly6C<sup>hi</sup> monocytes.

**Distinct gene profiles of F4/80<sup>hi</sup> and CD11b<sup>hi</sup> MΦ during ontogeny**

The results presented above suggested that microglia and F4/80<sup>hi</sup> MΦ from liver and kidney are derived from CD45<sup>+</sup>CX<sub>3</sub>CR1<sup>hi</sup>F4/80<sup>hi</sup>

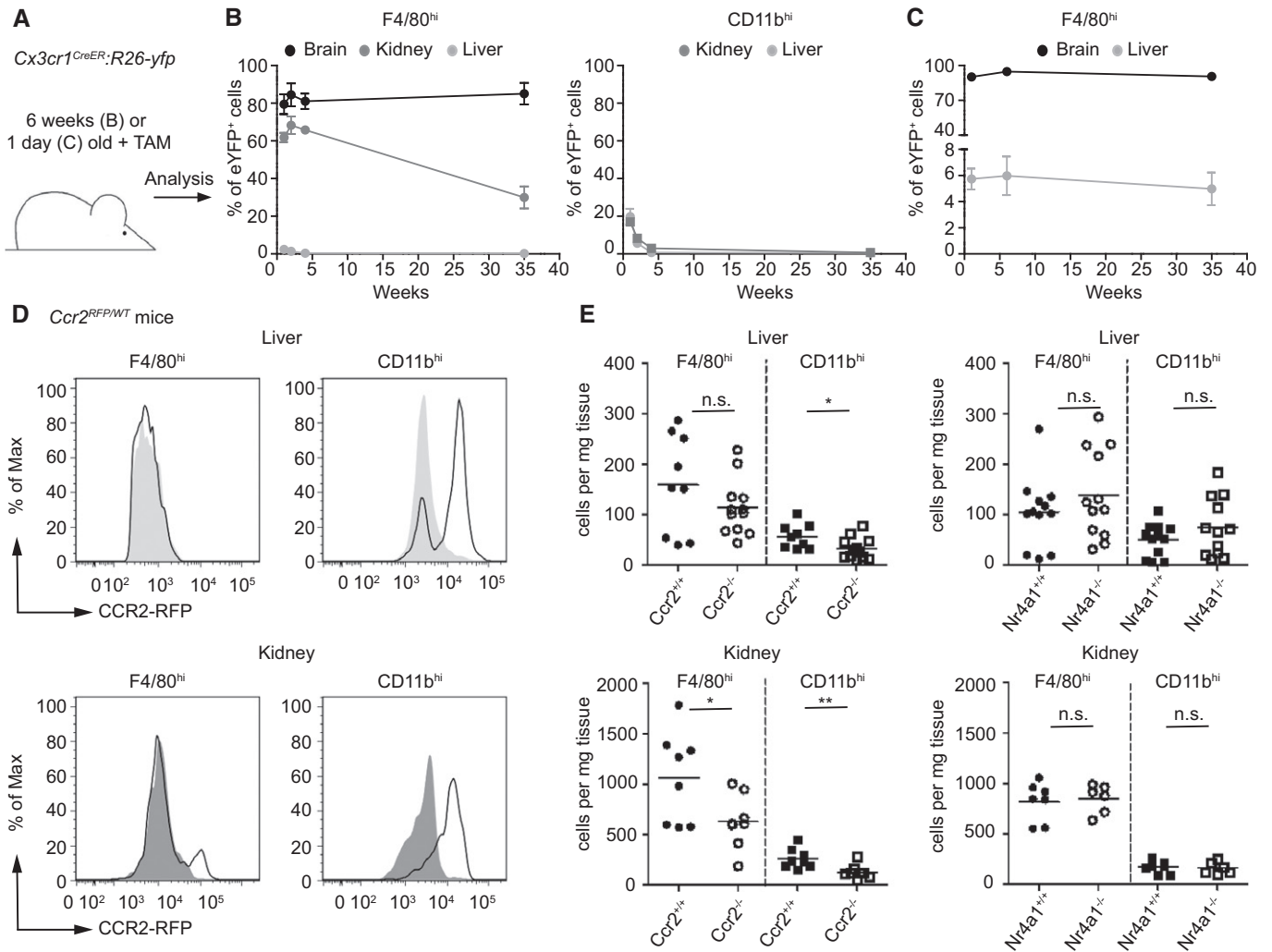


**Figure 2. Differences in turnover of CX<sub>3</sub>CR1<sup>+</sup> CD11b<sup>hi</sup> and F4/80<sup>hi</sup> tissue MΦ after birth.**

A Scheme of fate mapping in *Cx3cr1<sup>CreER</sup>;R26-yfp* mice that were either treated at 6 weeks of age (for B) or at postnatal day 1 (for C) and analyzed at 6 days, 2, 4, and 35 weeks (for B) and 6 days, 6 and 35 weeks (for C).

B, C Flow cytometric quantifications of YFP<sup>+</sup> MΦ in the brain, liver, and kidney at the indicated time points after TAM application in *Cx3cr1<sup>CreER</sup>;R26-yfp* mice. Data are summarized from two independent experiments (7–8 mice each) and represented as mean ± s.e.m.

D CCR2 expression on F4/80<sup>hi</sup> and CD11b<sup>hi</sup> MΦ in the liver or kidney of adult *Ccr2<sup>RFP/WT</sup>* mice, respectively. Gray area depicts fluorescence signal in MΦ of non-transgenic littermates. Representative cytometric graphs are shown. Four mice were investigated showing similar results.

E Flow cytometric analysis of MΦ populations in the liver or kidney in adult mice lacking *Ccr2* or *Nr4a1*. Each symbol represents one mouse. Data are summarized from three independent experiments and represent mean ± s.e.m. Significant differences were determined by an unpaired t-test. n.s.: not significant. \**P* < 0.05, \*\**p* < 0.01.

A2 progenitors in the YS, whereas CD11b<sup>hi</sup> MΦ seem to originate from later hematopoietic sources, for example, elements from the definitive hematopoiesis (Ginhoux & Jung, 2014). Thus, we examined whether this divergent origin is mirrored by a distinct gene profile. To do so, we performed an unsupervised clustering analysis of genomewide expression arrays from embryonic (Fig 3A) and adult (Fig 3B) F4/80<sup>hi</sup> MΦ in comparison with the CD11b<sup>hi</sup> populations. Hierarchical clustering based on the 1,010 most differentially expressed genes revealed that all F4/80<sup>hi</sup> MΦ in the brain, liver, and kidney shared a common signature of expressed genes, which was clearly distinct from the CD11b<sup>hi</sup> cells. Importantly, F4/80<sup>hi</sup> versus CD11b<sup>hi</sup> MΦ clustering was not only present prior to birth as

described recently (Schulz *et al*, 2012) but was still detectable in adulthood (Fig 3A and B). Based on the clear cut separation of F4/80<sup>hi</sup> versus CD11b<sup>hi</sup> MΦ by hierarchical cluster analyses, we created two groups, including only the embryonic or adult F4/80<sup>hi</sup> (microglia, liver and kidney) or CD11b<sup>hi</sup> (liver and kidney) MΦ and excluded genes that were significantly differentially expressed within one of the groups (Fig 3C and D). This approach confirmed the hypothesis of robust similarities within MΦ subgroups rather than within different MΦ populations in the same organ (Fig 3D). Notably, only adult Langerhans cells were transcriptionally separate from both adult F4/80<sup>hi</sup> and CD11b<sup>hi</sup> MΦ in other tissues emphasizing their distinct ancestry and kinetics compared to other MΦ as

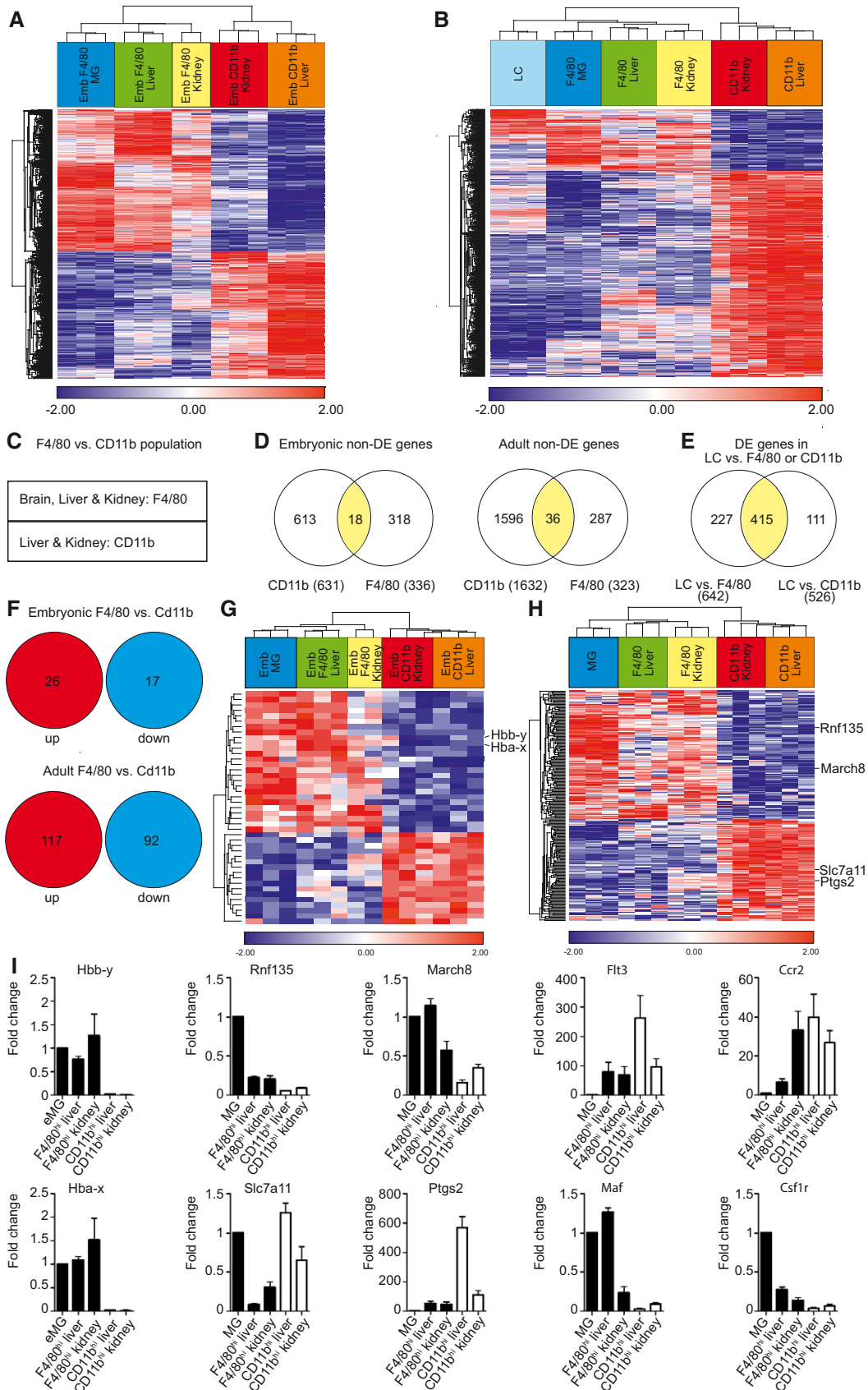


Figure 3.

**Figure 3. Distinct gene profile of F4/80<sup>hi</sup> and CD11b<sup>hi</sup> MΦ from embryogenesis until adulthood.**

- A Hierarchical clustering created on the 1,010 most significantly differentially expressed (DE) genes between embryonic (Emb) F4/80<sup>hi</sup> and CD11b<sup>hi</sup> cells. Heat map displays z-transformed log<sub>2</sub>-expression values from red to blue via white.
- B Hierarchical clustering based on the 755 most significantly differentially expressed genes between adult F4/80<sup>hi</sup> and CD11b<sup>hi</sup> cells. Heat map shows z-transformed log<sub>2</sub>-expression values from red to blue via white.
- C Scheme describing the compared samples of F4/80<sup>hi</sup> (microglia, liver, kidney) and CD11b<sup>hi</sup> (liver, kidney) tissue MΦ populations for analysis shown in (D–I).
- D Venn diagrams overlaying the genes which are jointly expressed in F4/80<sup>hi</sup> or in CD11b<sup>hi</sup> cells at similar levels irrespective of tissue origin (“non-differentially expressed (non-DE) genes”) defined by a false discovery rate (FDR) adjusted *P*-value > 0.95 for both embryonic and adult cells separately. Numbers in parentheses indicate the amount of all genes for each MΦ population.
- E Venn diagram shows the differentially expressed (DE) genes between adult Langerhans cells (LC) and adult F4/80<sup>hi</sup> or CD11b<sup>hi</sup> cells (functional connectivity |FC| > 1.5, FDR adjusted *P*-value < 0.05).
- F Number of up- and down-regulated genes in F4/80<sup>hi</sup> versus CD11b<sup>hi</sup> populations (|FC| > 1.5, FDR adjusted *P*-value < 0.05) from genes fulfilling the criteria in (D), that is, non-DE genes between organs for each group.
- G Hierarchical clustering of embryonic F4/80<sup>hi</sup> and CD11b<sup>hi</sup> cells based on 43 DE genes in embryonic cells visualized in (F). Heat map exhibits z-transformed log<sub>2</sub> expression values from red to blue via white.
- H Hierarchical clustering of adult F4/80<sup>hi</sup> and CD11b<sup>hi</sup> cells based on 209 DE genes in adult cells visualized in (F). Heat map presents z-transformed log<sub>2</sub> expression values from red to blue via white.
- I Quantitative RT–PCR of differentially expressed genes depicted in (G and H). Analyses of differentially expressed genes in embryonic (*Hbb-y* and *Hba-x*) or adult (*Rnf135*, *March8*, *Slc7a11*, *Ptgs2*, *Flt3*, *Ccr2*, *Maf*, and *Csf1r*) tissue macrophages. Data are normalized to β-actin and GAPDH and expressed as ratio of the mRNA expression compared to microglia and show mean ± s.e.m. Three mice per group were analyzed.

described before (Hoeffel *et al.*, 2012) (Fig 3B and E). Up- and down-regulated genes in F4/80<sup>hi</sup> versus CD11b<sup>hi</sup> MΦ were examined thoroughly (Fig 3F–I). The hemoglobin Y, beta-like embryonic chain (*Hbb-y*), and hemoglobin X, alpha-like embryonic chain in Hba complex (*Hba-x*), were highly enriched in embryonic F4/80<sup>hi</sup> MΦ of all tissues reflecting their common origin with erythrocytes from the EMP. Two E3 ubiquitin-protein ligases, namely *Rnf135* and *March8* that mediate ubiquitination of immune molecules such as CD86, MHC class II, and RIG-I, were more highly expressed in adult F4/80<sup>hi</sup> MΦ compared to CD11b<sup>hi</sup> MΦ. On the contrary, *solute carrier family 7, member 11* (*Slc7a11*), involved in the protection from oxidative stress, and *prostaglandin-endoperoxide synthase 2* (*Ptgs2*, also known as cyclooxygenase-2; *Cox-2*) involved in the regulation of inflammatory responses were highly up-regulated in adult CD11b<sup>hi</sup> MΦ. Additionally, adult CD11b<sup>hi</sup> MΦ were characterized by the enhanced expression of the chemokine receptor *Ccr2* and the growth factor *Flt3* that is present in multipotent hematopoietic progenitors. Complementary to the above data showing a contribution of Ly6C<sup>hi</sup> monocytes to F4/80<sup>hi</sup> kidney MΦ, *Ccr2* was also expressed in a high manner in this MΦ population. Long-living adult F4/80<sup>hi</sup> MΦ, however, expressed high levels of the transcription factor *Maf* and the macrophage colony-stimulating factor (*Csf1r*). We further visualized additional prominent examples of differentially expressed genes between F4/80<sup>hi</sup> and CD11b<sup>hi</sup> MΦ in different tissues during embryogenesis and adulthood related to macrophage function such as cytokines and other secreted proteins, antigen capturing molecules, proteolytic enzymes, cell surface markers, and transcription factors (Fig EV3 and Table EV1). Taken together, our observations suggest that a distinct genetic profile of F4/80<sup>hi</sup> and CD11b<sup>hi</sup> MΦ is present prenatally and in adulthood.

**Irf8 is expressed in F4/80<sup>hi</sup> and CD11b<sup>hi</sup> MΦ during ontogeny**

In addition to CSF-R1, several transcription factors such as PU.1 (encoded by *Sfpi*) and *Runx1* have been shown to be important for the lineage commitment in myeloid cells (Rosenbauer & Tenen, 2007). It is well established that PU.1 can act alone or in association with other transcription factors such as IRF8 (Rosenbauer & Tenen, 2007). To determine which transcription factors are present during

macrophage development, we measured *Runx1*, *Sfpi*, and *Irf8* levels in sorted EMP, A1 and A2 cells, embryonic microglia, and F4/80<sup>hi</sup> and CD11b<sup>hi</sup> MΦ from kidney and liver (Fig 4A). *Irf8* and *Sfpi* were barely detectable in EMP, whereas *Runx1* was strongly expressed. Notably, *Irf8*, *Runx1*, and *Sfpi* mRNA levels were continuously expressed during prenatal macrophage development, suggesting that these transcription factors play an important role for these macrophage populations. Since *Irf8* was described to play an essential role in the development of microglia, especially in the maturation of the A1 to A2 progenitor populations in the YS (Kierdorf *et al.*, 2013), we hypothesized that *Irf8* might also be required for other YS-derived F4/80<sup>hi</sup> MΦ populations. As expected, in the E 9.0 YS especially A2 cells expressed IRF8 as visualized in *Irf8*-VENUS PAC reporter mice (Fig 4B).

We next determined whether IRF8 expression is strictly developmentally regulated or whether it is also expressed in adult MΦ during homeostasis (Fig 4C and D). Microglia constantly expressed high levels of IRF8 from embryogenesis until adulthood (Fig 4C). Notably, CD11b<sup>hi</sup> and F4/80<sup>hi</sup> MΦ in the liver and kidney were strongly positive for the *Irf8*-VENUS signal suggesting an essential role of this transcription factor for MΦ maintenance.

**Irf8 regulates tissue MΦ homeostasis**

To assess the function of IRF8 in MΦ under steady-state conditions during adulthood, we used *Irf8*<sup>-/-</sup> mice to quantify the number of MΦ in brain, liver, and kidney and performed a thorough morphometric analysis of these cell populations (Fig 5). *Irf8*-deficient microglia exhibited drastic changes in their morphology including a significant decrease in their dendritic branching, assessed by filament length and number of dendrite terminal points per cell, whereas the cell number was increased (Fig 5A). Similarly, liver MΦ in *Irf8*<sup>-/-</sup> mice were characterized by a significantly reduced cell surface and volume as well as cell number (Fig 5B). In contrast, the number of kidney MΦ was significantly reduced by *Irf8* deficiency; the morphometric parameters, however, were unchanged (Fig 5C). Despite these severe effects on tissue MΦ, the organ function of the liver and kidney under homeostatic conditions was unimpaired in *Irf8*-deficient animals (Fig EV4).

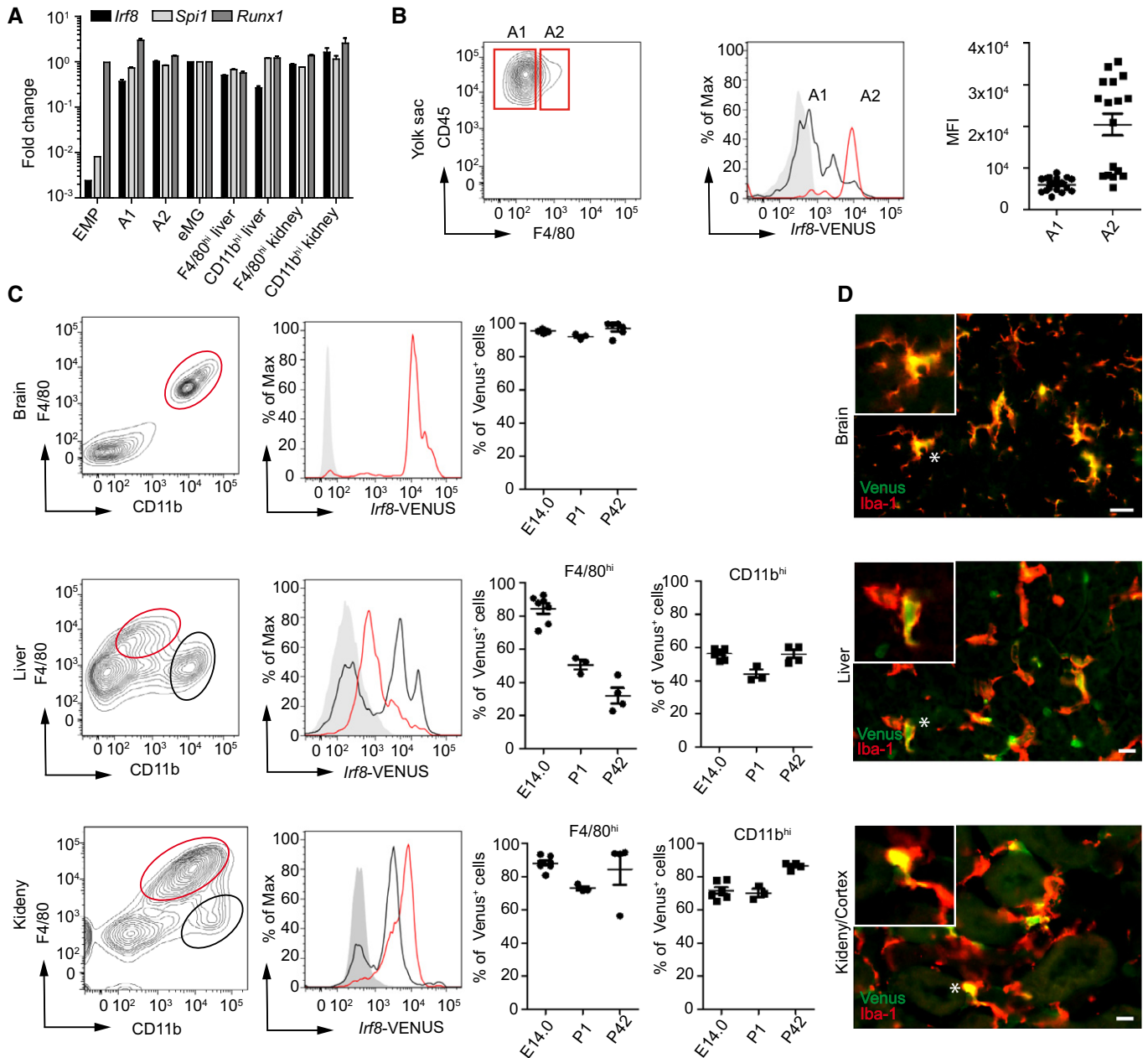


**Figure 4. *Irf8* is broadly expressed in tissue MΦ.**

A Quantitative qRT-PCR of transcription factors during MΦ development. Data are normalized to β-actin and GAPDH and expressed as ratio of the mRNA expression compared to embryonic microglia and show mean ± s.e.m. Two to three mice per group were analyzed.

B *Irf8*-Venus expression on A1 and A2 progenitor cells isolated from the E 9.0 yolk sac of *Irf8*-Venus PAC reporter mice. Representative blots obtained from 17 individual embryos are shown. Mean fluorescence intensity (MFI) of *Irf8*-Venus signal in A1 and A2 progenitor cells. Each symbol represents one mouse. Data are from one representative experiment out of two and represented as mean ± s.e.m.

C Flow cytometric measurement of the *Irf8*-Venus signal in brain, liver, and kidney MΦ from E 14.0, postnatal (P1), and adult (P42) *Irf8*-Venus PAC reporter mice. Representative density blots are shown (left) and quantification thereof (right). Each symbol represents one mouse. Data are from one representative experiment and displayed as mean ± s.e.m.

D Representative immunofluorescence images of Venus (green) and Iba-1<sup>+</sup> (red) MΦ from brain, liver, and kidney of adult *Irf8*-Venus PAC reporter mice. Stars indicate the cell shown in the insert. Scale bar represents 10 μm.

To further analyze the impact of *Irf8*-deficiency on tissue MΦ under homeostatic conditions, we performed a detailed transcriptional analysis. The number of differentially expressed genes between *Irf8*<sup>+/+</sup> and *Irf8*<sup>-/-</sup> mice was higher in the embryonic

compared to the adult MΦ cell populations (Fig 6A). Moreover, *Irf8* deficiency had an influence on the transcriptional pattern of both F4/80<sup>hi</sup> and CD11b<sup>hi</sup> MΦ populations (Fig 6A–C). The genes commonly up- (red) or down (blue)-regulated in embryonic and



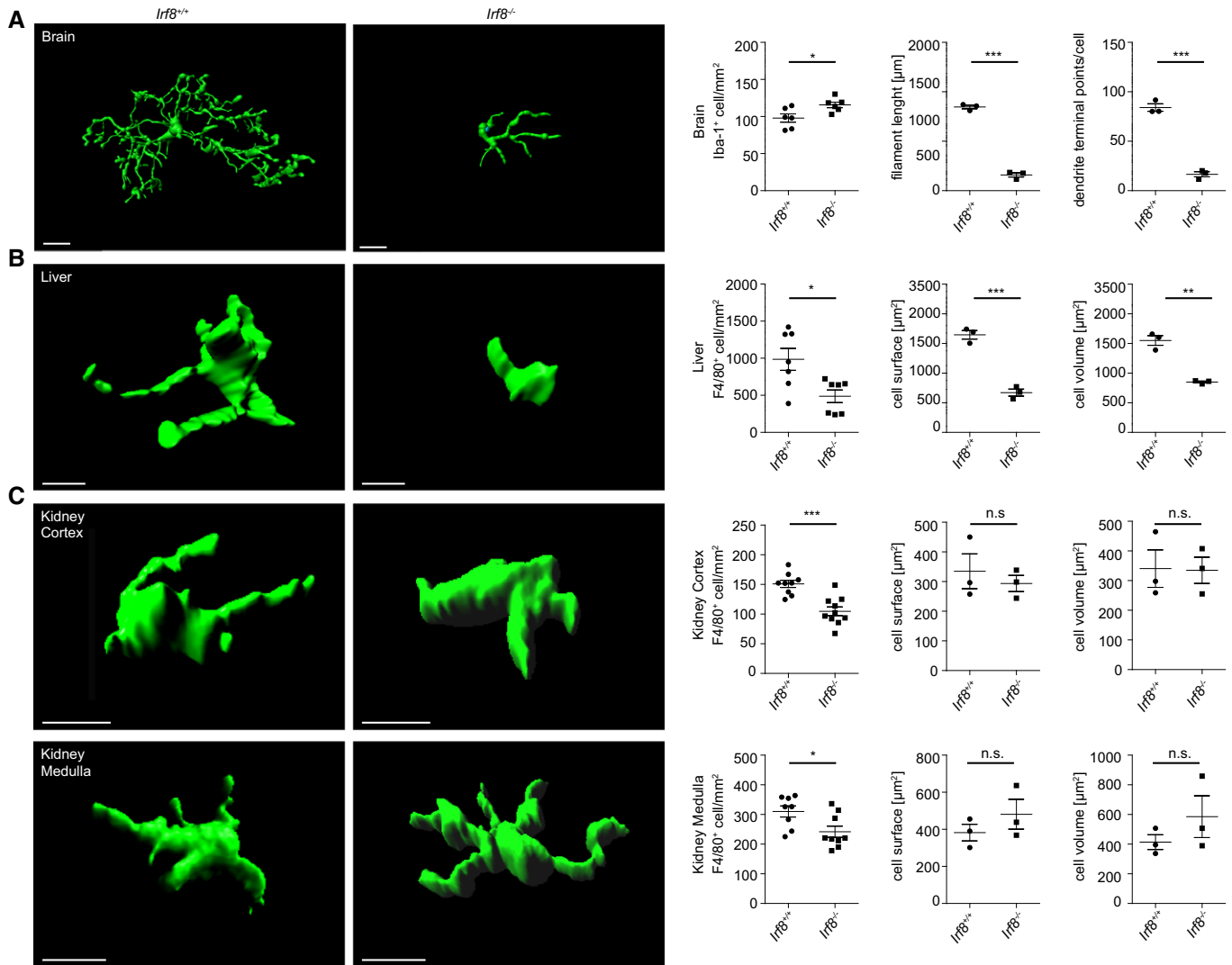


**Figure 5. Lack of *Irf8* impairs tissue MΦ homeostasis.**

A–C Three-dimensional reconstruction (left) and Imaris-based morphometric analysis of CX3CR1<sup>+</sup> brain microglia or F4/80<sup>+</sup> liver and kidney MΦ in adult *Irf8*<sup>-/-</sup> or *Irf8*<sup>+/+</sup> mice, respectively. Quantification of cell density of Iba-1<sup>+</sup> microglia and F4/80<sup>+</sup> liver and kidney MΦ in adult *Irf8*<sup>-/-</sup> or *Irf8*<sup>+/+</sup> mice, respectively (left). Scale bars represent 10 μm. For morphological measurements, each symbol represents one mouse with at least six examined cells per mouse. Data represent mean ± s.e.m. Significant differences were examined by an unpaired *t*-test and marked with asterisks (\**P* < 0.05, \*\**P* < 0.01, \*\*\**P* < 0.001); n.s.: not significant.

adult CD11b<sup>hi</sup> or F4/80<sup>hi</sup> MΦ populations exhibited distinct gene ontology (GO) clusters (Fig 6D). Obviously, genes related to the immune system were down-regulated in all *Irf8*<sup>-/-</sup> MΦ populations suggesting an impact of IRF8 on the immune response of these cells. Quantitative RT-PCR performed with the adult MΦ populations confirmed this finding by showing a down-regulation of *Toll-like receptor 12* (*Tlr12*), *major histocompatibility complex class II, DM alpha* (*H2-DMa*), and *basic leucine zipper transcription factor and ATF-Like 3* (*Batf3*) in *Irf8*<sup>-/-</sup> F4/80<sup>hi</sup> MΦ (Fig 6E). Moreover, *Cd36*, *Fc fragment of IgG, high affinity Ia, receptor* (*Fcgr1* also known as *Cd64*), and *Irf7* were down-regulated in *Irf8*<sup>-/-</sup> CD11b<sup>hi</sup> MΦ (Fig 6E). All of these genes are involved in immune response or regulation of type I interferons. Suppression of MHC class II expression on *Irf8*<sup>-/-</sup> MΦ was additionally confirmed by immunohistochemistry (Fig EV5). In sum, these data provide clear evidence for an essential role of IRF8

for ensuring proper MΦ maturation throughout development and adulthood in both F4/80<sup>hi</sup> and CD11b<sup>hi</sup> MΦ.

## Discussion

Herein we describe, based on a novel fate-mapping system using *Cx3cr1*<sup>CreER</sup> mice to specifically target A2 progenitors in the YS, the origin and turnover as well as the unique transcriptional pattern of F4/80<sup>hi</sup> and CD11b<sup>hi</sup> MΦ in the liver, kidney, brain, and epidermis and thereby identified *Irf8* as an important transcription factor for proper MΦ maturation.

To date, F4/80<sup>hi</sup> MΦ were mainly believed to be YS-derived, whereas CD11b<sup>hi</sup> MΦ were shown to originate from the definitive hematopoiesis (Schulz *et al*, 2012; Gomez *et al*, 2015). However,

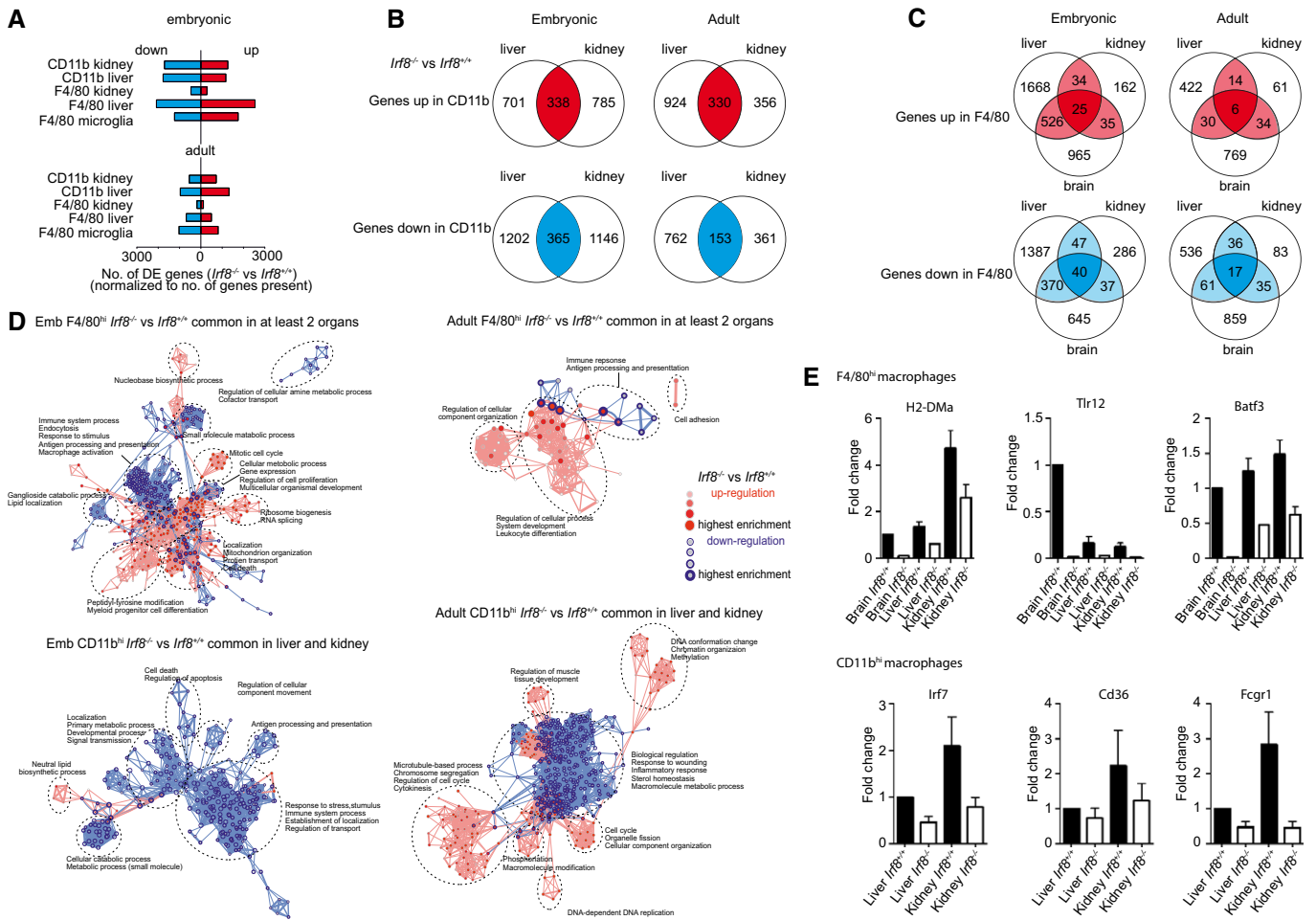


**Figure 6. Altered gene transcription profile in MΦ lacking *Irf8*.**

**A** Number of differentially expressed (DE) genes between *Irf8*<sup>+/+</sup> and *Irf8*<sup>-/-</sup> mice in several embryonic and adult MΦ cell populations. DE genes were identified by a one-way ANOVA model ( $|FC| > 1.5$ , FDR adjusted  $P$ -value  $< 0.05$ ). The absolute numbers were normalized to the number of genes present in embryonic or adult cells.

**B** Venn diagrams of DE genes between *Irf8*<sup>+/+</sup> and *Irf8*<sup>-/-</sup> CD11b<sup>hi</sup> cells from adult or embryonic liver and kidney. Commonly up- (red area) and down-regulated (blue area) genes between cells derived from *Irf8*<sup>+/+</sup> and *Irf8*<sup>-/-</sup> mice are shown.

**C** Venn diagrams of DE genes for F4/80<sup>hi</sup> cells from adult or embryonic liver, kidney, and brain. Commonly up- (red area) and down-regulated (blue area) genes are shown.

**D** Gene Ontology (GO) network built on common DE genes in embryonic (left panel) and adult (right panel) F4/80<sup>hi</sup> (upper row) CD11b<sup>hi</sup> (lower row) cells from microglia, liver, and kidney identified in at least two organs (identified in B and C). Red symbols represent GO terms associated with up-regulated genes in *Irf8*<sup>-/-</sup> compared to *Irf8*<sup>+/+</sup> mice, while blue edges indicate down-regulation.

**E** Quantitative qRT-PCR of selected genes in tissue MΦ from adult *Irf8*<sup>-/-</sup> and *Irf8*<sup>+/+</sup> mice. Data are normalized to  $\beta$ -actin and GAPDH and expressed as ratio of the mRNA expression compared to microglia of *Irf8*<sup>+/+</sup> mice or to liver CD11b<sup>hi</sup> cells of *Irf8*<sup>+/+</sup> mice and show mean  $\pm$  s.e.m. Three mice per group were analyzed.

this view was recently challenged by a study claiming that only microglia are YS-derived, whereas all other tissue MΦ are fetal liver-derived (Sheng *et al*, 2015). In contrast, our data do not support the idea of a complete fetal liver origin of all tissue F4/80<sup>hi</sup> MΦ except microglia but instead confirm earlier reports on the YS origin of most F4/80<sup>hi</sup> tissue MΦ (Schulz *et al*, 2012; Gomez *et al*, 2015). These studies provided clear evidence that EMPs, localized in the YS, are the non-committed progenitors of tissue MΦ. Our own data add exciting new facets to the YS origin of tissue MΦ. Using a new fate-mapping strategy in *Cx3cr1*<sup>CreER</sup>:*Rosa26-ypf* mice combined with transcriptional analysis, we place the A2-progenitor population of the YS as the direct precursors of microglia and partially F4/80<sup>hi</sup> MΦ in the liver and kidney as well as Langerhans cells. By confocal

microscopy of E 9.0 and E 10.0/10.5 embryos and the E 9.0 YS, we proved that CX<sub>3</sub>CR1<sup>+</sup> cells are exclusively present in the YS but not in the P-Sp/AGM or fetal liver at these time points and are therefore the only progenitor cells which are targeted by our fate-mapping strategy. Additionally, our results show that, except for microglia, the YS-derived F4/80<sup>hi</sup> MΦ population in the liver and kidney as well as Langerhans cells was decreased during development suggesting a second source for these cell populations. These data support the previous findings that YS-derived Langerhans cell precursors are potentially replaced by fetal liver-derived HSCs and therefore present the main source of the adult Langerhans cells (Hoeffel *et al*, 2012). Our results suggest a similar scenario for adult F4/80<sup>hi</sup> MΦ in kidney and liver. In contrast, CD11b<sup>hi</sup> MΦ in

liver and kidney were not targeted by our fate-mapping strategy demonstrating their origin from definitive hematopoiesis. Our data stand in contrast to a recent publication, which claims an exclusive origin of all M $\Phi$  from the fetal liver (Sheng *et al*, 2015). Even though a contribution of bone marrow-derived HSCs to F4/80<sup>hi</sup> kidney M $\Phi$  was previously suggested (Schulz *et al*, 2012), the maintenance and turnover of these cells as well as of F4/80<sup>hi</sup> Kupffer cells and CD11b<sup>hi</sup> liver M $\Phi$  were so far not investigated. Using adult *Cx3cr1<sup>CreER</sup>:Rosa26-yfp* mice, we could identify a low but constant turnover rate for F4/80<sup>hi</sup> kidney M $\Phi$  in contrast to a high turnover rate for CD11b<sup>hi</sup> M $\Phi$ . To bypass the down-regulation of CX<sub>3</sub>CR1 expression in F4/80<sup>hi</sup> Kupffer cells during postnatal life, we directly targeted these cells after birth. So far, it was only shown indirectly that Kupffer cells have apparently no contribution from blood monocytes using either *Ccr2*-deficient (Bain *et al*, 2014) or parabiotic mice under homeostatic conditions (Epelman *et al*, 2014). However, a contribution of blood monocytes to F4/80<sup>hi</sup> Kupffer cells under disease conditions or after depletion was recently suggested (Bleriot *et al*, 2015; Scott *et al*, 2016). Our results provide therefore the first direct genetic proof that at least a subpopulation of the Kupffer cells has no turnover from birth until 9 months of age under steady-state conditions. Recently, *Clec4* has been identified as a specific gene for Kupffer cells (Scott *et al*, 2016) and this might open new possibilities to further study explicitly this cell population in future.

A broad transcriptional analysis of different tissue M $\Phi$  populations revealed that M $\Phi$  gene expression is strongly dependent on the specific organ environment (Gautier *et al*, 2012). Moreover, separation of embryonic F4/80<sup>hi</sup> and CD11b<sup>hi</sup> tissue M $\Phi$  by gene expression pattern was previously suggested (Schulz *et al*, 2012). In the present study, we additionally performed transcriptional microarray analysis of embryonic and adult F4/80<sup>hi</sup> and CD11b<sup>hi</sup> tissue M $\Phi$  including microglia and adult Langerhans cells. Despite organ-specific expression patterns (data not shown), we identified robust similarities of F4/80<sup>hi</sup> versus CD11b<sup>hi</sup> M $\Phi$  across organs which were present prenatally and in adulthood. Interestingly, only Langerhans cells were transcriptionally separated from both the adult F4/80<sup>hi</sup> and CD11b<sup>hi</sup> M $\Phi$  indicating that they represent a unique tissue M $\Phi$  population. Of note, we defined signature genes for tissue macrophages based on a previous analysis (Lavin *et al*, 2014) using linear support vector regression implemented in CIBERSORT (Newman *et al*, 2015) and could demonstrate that microglia and Kupffer cells in our analysis were mainly characterized by the same signature genes (data not shown). This suggests that our sorting strategy was compatible with previous approaches to determine tissue macrophages.

PU.1 has been described as a key regulator of myeloid/macrophage development for a long time, reflected by a complete absence of mature macrophages in Pu.1-deficient animals (McKercher *et al*, 1996). In contrast, *Irf8* was only described as a transcription factor regulating myeloid and lymphoid maturation (Holtschke *et al*, 1996; Hambleton *et al*, 2011). More recently, we described that *Irf8* is essential for the maturation of the YS A1- to A2-progenitor populations (Kierdorf *et al*, 2013; Shiao *et al*, 2015). The importance of *Irf8* for microglia from the early wave of hematopoiesis was also observed in zebrafish (Shiao *et al*, 2015). Interestingly, in their study, the impact on peripheral M $\Phi$  was limited to the embryonic stage, whereas the effect on microglia was long-lasting. However,

the role of *Irf8* for other murine tissue M $\Phi$  was not studied so far. Therefore, we analyzed if the YS-derived F4/80<sup>hi</sup> tissue M $\Phi$  are dependent on the transcription factor *Irf8* concerning maturation and homeostasis. Surprisingly, we identified a remarkably high expression of *Irf8* in both F4/80<sup>hi</sup> and CD11b<sup>hi</sup> M $\Phi$  and indeed found an impact of *Irf8* on cell morphology and/or cell number of all tissue M $\Phi$ . Moreover, *Irf8* deficiency showed considerable impact on the gene expression profile of F4/80<sup>hi</sup> and CD11b<sup>hi</sup> M $\Phi$  derived from all organs and both during embryogenesis and adulthood leading to the down-regulation of genes related to immune function. In summary, we report that F4/80<sup>hi</sup> tissue M $\Phi$  are A2 YS progenitor-derived, whereas CD11b<sup>hi</sup> tissue M $\Phi$  are exclusively derived from the definitive hematopoiesis independent from A2 precursors. Furthermore, we identified distinct gene profiles of the two tissue M $\Phi$  populations. We were, for the first time, able to analyze the turnover rate of tissue M $\Phi$  in the liver and kidney and show a low but constant turnover rate of F4/80<sup>hi</sup> kidney M $\Phi$ , a high turnover rate for CD11b<sup>hi</sup> tissue M $\Phi$ , and no turnover of F4/80<sup>hi</sup> liver M $\Phi$ . Moreover, we found that *Irf8* is crucial for proper maturation of microglia as well as liver and kidney M $\Phi$ .

## Materials and Methods

### Mice

*Cx3cr1<sup>GFP/WT</sup>*, *Cx3cr1<sup>CreER</sup>:R26-yfp* (Jung *et al*, 2000; Yona *et al*, 2013), *Ccr2<sup>-/-</sup>* (Boring *et al*, 1997), *Nr4a1<sup>-/-</sup>*, *Irf8<sup>-/-</sup>* (Holtschke *et al*, 1996); *Irf8*-VENUS (Schonheit *et al*, 2013) *Ccr2<sup>RFP/WT</sup>* were described elsewhere. All mice including the corresponding wild-type controls were bred in-house and were housed in specific pathogen-free conditions. Experiments were performed with 6- to 10-week-old female and male mice, if not stated otherwise. All mouse experiments were performed in accordance with the animal law and guidelines. PAC-transgenic *Irf8*-Venus mice were kindly provided by Frank Rosenbauer (Medical Faculty of the WWU Münster, Germany), *Nr4a1<sup>-/-</sup>* mice by Antigoni Triantafyllou (University Hospital Freiburg, Germany), and *Ccr2<sup>RFP/WT</sup>* mice by Mathias Jucker (German Center for Neurodegenerative Diseases, Tübingen, Germany).

### Timed matings

Timed matings were used to analyze embryonic mice. The matings were started in the afternoon and separated after plug check on the following morning. Embryonic development was estimated considering the day of vaginal plug formation as embryonic day (E) 0.5 and staged by developmental criteria. The EMP was isolated at E 8.0, A1 and A2 at E 9.0, embryonic macrophage populations at E 14.5, and adult macrophage populations at postnatal day (P)42.

### Tamoxifen induction

Tamoxifen (TAM, Sigma-Aldrich, Taufkirchen, Germany) was dissolved in corn oil (Sigma-Aldrich, Taufkirchen, Germany) to get a 20 mg/ml solution for injections. Six-week-old *Cx3cr1<sup>CreER</sup>:Rosa26-yfp* mice were subcutaneously injected with 4 mg TAM on

2 days (day 0 and 2). For Cre induction in the newborn mice, intraperitoneal (i.p.) injection of 0.1 mg TAM was performed at P1. For pulse labeling experiments, plug-positive *Cx3cr1<sup>CreER</sup>*:*Rosa26-yfp* females from timed matings were i.p. injected with 3 mg TAM (20 mg/ml TAM + 10 mg/ml Progesterone; Sigma-Aldrich, Taufkirchen, Germany) at E 9.0, E 8.0, or E 7.0.

### Preparation of tissue samples

Mice were lethally anesthetized with ketamine (100 mg/kg bodyweight, Medistar, Germany) and xylazine (5 mg/kg bodyweight, Bayer, Leverkusen, Germany) followed by the perfusion with 1× PBS through the left heart chamber. For histology, organs were transferred to 4% PFA. For the preparation of single-cell suspension for flow cytometry, brain, liver, and kidney were cut into small pieces. The tissue of the liver and kidney was transferred to enzymatic solutions (1 mg/ml collagenase D (Roche, Darmstadt, Germany) + 2.4 mg/ml dispase (Roche, Darmstadt, Germany) + 0.2 mg/ml DNase (Sigma-Aldrich, Taufkirchen, Germany) in 1× PBS for the liver and 1 mg/ml collagenase D in 1× PBS for the kidney) and incubated for 30 min at 37°C on a shaker. Cell suspensions were filtered through a mesh (100 or 70 µm, restrictively). The liver samples were centrifuged at 54 g for 3 min, 4°C. Supernatant was transferred to a new tube. Liver and kidney samples were centrifuged for 5 min 251 g, 4°C. Erythrocytes were removed by RBC lysis buffer (eBioscience, San Diego, USA). Brain tissue was homogenized and filtered through a 70 µm mesh. After centrifugation (10 min 251 g, 4°C), the pellet was resuspended in 70% Percoll (Sigma-Aldrich, Taufkirchen, Germany) and was underlay to a Percoll density gradient (30 and 37%). Density gradient centrifugation was performed for 30 min, 800 g at 4°C without brake. Microglia were collected from the interphase 70% to 37% Percoll. For skin samples, ears were separated and dermis was put on a 0.2 mg/ml dispase solution o/n 4°C, dermis and epidermis were separated, and the epidermis was cut in small pieces followed by enzymatic (1.5 mg/ml collagenase V, Life technologies, Darmstadt, Germany) digestion for 1.5 h at 37°C. Homogenates were filtered through a 100 µm mesh and centrifuged (251 g, 5 min, 4°C). Cell suspensions from isolated YS were obtained by mechanical homogenization, using passage through 22–25 gauge needles as described before (Bertrand *et al*, 2005).

### Flow cytometry

Cells were acquired on FACSCanto II and LSRFortessa systems (BD Bioscience, Heidelberg, Germany) and analyzed with Flowjo software (TreeStar). Cell sorting was performed on a MoFlo Astrios (Beckman Coulter, Krefeld, Germany). The following antibodies were used for staining cells: anti-CD45 (clone 30-F11, eBioscience, San Diego, USA), anti-CD11b (clone M1/70, eBioscience, San Diego, USA), anti-CD146 (clone ME-9F1, Biolegend, Fell, Germany), anti-CD3 (clone eBio500A2, eBioscience, San Diego, USA), anti-CD19 (clone eBio1D3, eBioscience, San Diego, USA), anti-NK1.1 (clone PK136, eBioscience, San Diego, USA), anti-Gr1 (clone RB6-8C5, Biolegend, Fell, Germany), anti-F4/80 (clone BM8, eBioscience), anti-MHCII (clone M5/114.15.2, eBioscience, San Diego, USA), anti-EpCAM (clone G8.8, BD Bioscience, Heidelberg, Germany), and anti-Ly6C (clone AL 21, BD Bioscience,

Heidelberg, Germany). Before surface staining, dead cells were stained using the Fixable Viability Dye eFluor<sup>®</sup> 780 or eFluor<sup>®</sup> 506 (eBioscience, San Diego, USA) followed by incubation with Fc receptor blocking antibody CD16/CD32 (clone 2.4G2, BD Bioscience, Heidelberg, Germany).

The turnover rate per week was calculated as following: For CD11b<sup>hi</sup> MΦ, the difference of YFP<sup>+</sup> CD11b<sup>hi</sup> MΦ at 6 days to YFP<sup>+</sup> CD11b<sup>hi</sup> MΦ at 4 weeks was defined. This value was calculated per week and then given as % of YFP<sup>+</sup> CD11b<sup>hi</sup> MΦ at 6 days. The same calculation was done for kidney F4/80<sup>hi</sup> MΦ using the 2-week and 35-week time point.

### Histology

For whole embryo imaging, E9.0 *Cx3Cr1<sup>GFP/+</sup>* embryos were fixed for 10 min in 4% paraformaldehyde and processed for whole-mount immunolabeling, using F4/80-APC (Clone BM8, eBioscience, San Diego, USA) or c-kit-APC (Clone 2B8, eBioscience, San Diego, USA), CD41-AF647 (Clone eBioMWRreg30, Molecular Probes, Eugene, Oregon, USA), and CD31-PE (Clone Mec13.3, BioLegend, Fell, Germany) antibodies, as previously described (Bertrand *et al*, 2005). Whole embryos or isolated YS were placed in the central well of glass bottom culture dishes (P35G-1.5-10-C, from MatTek, USA) filled with PBS + 10% fetal calf serum. After appropriate orientation of the sample, the well was covered with a 12-mm coverslip glass. Image stacks were collected using a Leica SP8 confocal microscope. Images were processed using Fiji and PHOTOSHOP 8.0 (Adobe Systems, San Jose, CA) software.

For immunofluorescence staining with cryosections, tissues were fixed overnight at 4°C, dehydrated in 30% sucrose solution, and embedded in Tissue-Tek<sup>®</sup> O.C.T.TM Compound (Sakura Finetek Europ B.V., Netherlands); 12- or 30-µm parasagittal sections were cut on a cryotome and mounted onto microscope slides (Langenbrinck, Emmendingen, Germany) for staining. The organ slices were fixed in acetone for 20 min at –20°C and rehydrated in PBS. Blocking was performed with 5% BSA, 0.1% Triton X-100 in PBS for 1 h. The 12-µm sections were incubated with the primary antibodies anti-GFP (1:1,000, Cat. No. 600-101-215S, Rockland, Limerick, USA) and anti-Iba1 (1:500, Cat. No. 019-19741, Wako, Osaka, Japan) in 1% BSA in PBS at 4°C overnight, whereas 30-µm sections were incubated with anti-F4/80 (1:200, Cat. No. MCA-497, Serotec, Düsseldorf, Germany) or anti-Iba1 for two nights followed by the incubation with the secondary antibodies (Alexa Fluor 555, Alexa Fluor 647 or Alexa Fluor 488, 1:500, Life technologies, Darmstadt, Germany) in 1% BSA in PBS for 1 h at RT in the dark. Nuclei were counterstained with 4,6-diamidino-2-phenylindole (DAPI, 1:10,000, Cat. No. 236276, Boehringer, Mannheim, Germany) for 10–15 min, and the slides were mounted using Mowiol (Merck Millipore, Darmstadt, Germany). Representative pictures were taken with BZ-9000 Biorevo microscope (Keyence, Neu-Isenburg, Germany).

### Imaris reconstruction

3D reconstruction of tissue macrophages was done using the IMARIS software (Bitplane, Zürich, Switzerland) as described previously (Erny *et al*, 2015). In brief, F4/80 or Iba-1 immunostained 30-µm cryosections from adult brain, liver, and kidney

were used. Imaging was performed on an Olympus Fluoview 1000 confocal laser scanning microscope (Olympus, Hamburg, Germany) using a  $20 \times 0.95$  NA objective. Z stacks were done with  $3 \times$  zoom in  $1.14 \mu\text{m}$  steps in z direction;  $1,024 \times 1,024$  pixel resolution was recorded and analyzed using IMARIS software (Bitplane, Zürich, Switzerland). At least six  $\text{F4/80}^+ \text{GFP}^+$  cells were reconstructed per analyzed mouse using the surface plug-in on the GFP or F4/80 signal.

### Microarray analysis

FACS-sorted M $\Phi$  populations were directly collected in cell lysis buffer, and subsequently, RNA was isolated with the Arcturus Pico Pure RNA Isolation Kit (Life technologies, Darmstadt, Germany) according to the manufacturer's protocol. Transcriptional profiles of the M $\Phi$  populations were assessed using Affymetrix<sup>®</sup> (Affymetrix, Santa Clara, USA) GeneChip Arrays (Mouse Gene 2.1 ST Arrays). Affymetrix<sup>®</sup> GeneChip array data were pre-processed using Affymetrix<sup>®</sup> Expression Console and normalized through the Robust Multi-array Average (RMA) implementation in the Expression Console. Sample processing and Affymetrix microarray hybridization were carried out at a genomics core facility: Center of Excellence for Fluorescent Bioanalytics (KFB, University of Regensburg, Germany).

### Pre-processing of gene expression data

The Robust Multi-array Average (RMA) function was used to normalize the data during import of the raw Affymetrix data (CEL files) of a total of 81 samples into Partek Genomics Suite (PGS). The background value was defined as the median of the entire normalized dataset using all probes. Gene probes were only kept for further analysis if their mean expression values were higher than the background in at least one group or condition within the whole dataset. Next, multiple probes for one gene locus were filtered allowing only one probe with the highest overall mean expression. These pre-processing steps resulted in 17,888 unique genes to be present in at least one group or condition. These genes were retained for further analyses.

### Identification of differentially expressed genes and hierarchical clustering

Differentially expressed (DE) genes were defined in PGS by analysis of variance (ANOVA) models by setting certain fold change (FC) thresholds and false discovery rate [FDR, (Hochberg & Benjamini, 1990)] adjusted *P*-value cutoffs to determine differences between two comparable groups, for example, cells derived from *Irf8*<sup>-/-</sup> versus *Irf8*<sup>+/+</sup> mice. The respective cutoffs used for a particular comparison are described in the result section. For comparison of DE genes between different pairs of cell populations, we applied Venn diagrams. When comparing all cell populations between *Irf8*<sup>-/-</sup> versus *Irf8*<sup>+/+</sup> mice, the absolute numbers of up- and down-regulated genes from each cell population were normalized to the number of present genes and then visualized as bar plots. The most variable genes were determined in ANOVA models to compare the variations throughout groups by *t*-test, that is, genes with most significant *P*-values. Hierarchical clustering using the Euclidean

distance on both genes and samples was performed and used for visualization of DE genes between or most variable genes of particular cell populations.

### Visualization of differentially expressed genes related to macrophage function

The differentially expressed genes comparing *F4/80*<sup>hi</sup> against *CD11b*<sup>hi</sup> in adult (755 DE genes) and embryo (1,010 DE genes) were filtered by a list of known murine cytokines (233 cytokines), by a list of antigen capturing molecules (34 molecules [Scavenger receptors in homeostasis and immunity] [Myeloid C-type Lectin Receptors in Pathogen Recognition and Host Defense]), by a list of proteolytic enzymes (754 enzymes [Twenty years of the MEROPS database of proteolytic enzymes, their substrates and inhibitors. Nucleic Acids Res 44, D343-D350]), by a list of surface markers (3,705 marker), by a list of transcription factors (929 factors [The TRANSFAC project as an example of framework technology that supports the analysis of genomic regulation]), and by a list of secreted molecules (1,139 molecules). Only the top 10 genes among the differentially expressed molecules from the above mentioned categories were visualized in a heat map using Mayday-Integrative Analytics for Expression Data (Battke *et al.*, 2010). The top 10 genes were selected by the highest FC comparing *F4/80*<sup>hi</sup> against *CD11b*<sup>hi</sup> in adult and embryo for each category, respectively.

### Co-regulation analysis by BioLayout Express3D

BioLayout Express3D (BioLayout) is a powerful tool for the visualization and analysis of network graphs based on co-expression (Theocharidis *et al.*, 2009). BioLayout was applied to discriminate different cell populations during embryonic M $\Phi$  development. Sample-sample correlation was calculated and transformed into 3D coordinates. A Pearson's correlation coefficient cutoff of 0.92 was used to keep stronger connections (higher correlation) between samples, and subsequently, the co-regulation network was constructed and visualized in 3D space.

Gene Ontology (GO) enrichment analysis and GO network visualization. To link the data to prior knowledge, GO enrichment analysis was applied by using the Cytoscape plug-in BiNGO (v2.44) (Maere *et al.*, 2005). To include only significant results, the FDR *q*-value threshold was set to 0.05 as default. The Cytoscape plugins Enrichment Map (v1.1) (Merico *et al.*, 2010) and Word Cloud (Oesper *et al.*, 2011) were used to visualize the GO networks. To decrease the size of the networks and to define certain cutoffs for the similarity of GO terms, the default settings of Jaccard coefficients (0.25) and their FDR *q*-values (0.1) were utilized.

### PCR array

For quantitative gene expression analysis, the RNA of FACS-sorted M $\Phi$  population was isolated as described above. Reverse transcription was performed using the RT<sup>2</sup> PreAMP cDNA Synthesis Kit (Qiagen, Germantown, USA) with a custom-made Primer-Mix according to manufacturer's instructions. RT-PCR was performed using a custom-made SABioscience PCR-Array (Qiagen, Germantown, USA) with the genes of interest and analyzed with a LightCycler 480 (Roche, Darmstadt, Germany). Beta-Actin and GAPDH were used as

housekeeping genes. Analysis was performed using the online data analysis center from Qiagen.

### Serum protein quantifications

Serum ALT was analyzed from whole blood using ALT strips from Roche according to the manufacturer's instructions. Measurement was performed in a Reflovet machine from SCIL animal care. Values above assay range were diluted prior to measurement. Serum creatinine was measured using an enzymatic colorimetric (ELISA) creatinine kit (Lehmann) following the manufacturer's instructions.

### Bacterial load

Liver lobes from adult *Irf8*<sup>-/-</sup> and *Irf8*<sup>+/+</sup> were dissected and weighted before bacterial DNA was isolated from the livers as described before (Wilson & Grenfell, 1997). Quantitative PCR for 16sRNA gene was performed and normalized to the weight of the isolated tissue.

### Statistical analysis

Statistical analysis was performed using GraphPad Prism (GraphPad Software, Version 6.0, La Jolla, USA). All data were tested for normality applying the *F*-test to compare variance. If normality was given, an unpaired *t*-test, two-sided was applied. If the data did not meet the criteria of normality, the Mann–Whitney *U*-test, two-sided was applied. Differences were considered significant when *P*-value < 0.05.

### GEO accession numbers

The main GEO accession number for microarray: GSE73125.

**Expanded View** for this article is available online.

### Acknowledgements

We thank Maria Oberle and Fleur Feder for excellent technical assistance, Ori Staszewski for statistical advice, Antigoni Triantafyllou for providing *Nr4a1*<sup>-/-</sup> mice, Mathias Jucker for providing *Ccr2*<sup>RFP/WT</sup> mice, and Stefanie M. Brendecke for critically reading and editing the manuscript. MP was supported by the BMBF-funded competence network of multiple sclerosis (KKNMS), the Sobek Foundation, the DFG (SFB 992, SFB 1160, FOR1336, PR 577/8-1), the Fritz-Thyssen Foundation, the Gemeinnützige Hertie Foundation (GHST) and the SFB(CRC)/TRR 167. JLS is a member of the Excellence Cluster ImmunoSensation, and he was supported by the DFG (SFB 645, SFB 704).

### Author contributions

NH, KK, ZA, MR, and KF conducted the experiments. JX, TU, and JLS analyzed the microarray data. IG performed immunofluorescence analysis of the YS and embryo at E 9.0. PW, MJCJ and GY performed the 3D reconstruction of *Irf8*<sup>-/-</sup> and *Irf8*<sup>+/+</sup> microglia and liver macrophages and the quantification thereof. FR provided *Irf8*-VENUS mice; MH and PAK designed experiments. JLS supported writing the manuscript. MP and NH supervised the project and wrote the manuscript.

### Conflict of interest

The authors declare that they have no conflict of interest.

## References

- Ajami B, Bennett JL, Krieger C, Tetzlaff W, Rossi FM (2007) Local self-renewal can sustain CNS microglia maintenance and function throughout adult life. *Nat Neurosci* 10: 1538–1543
- Bain CC, Bravo-Blas A, Scott CL, Gomez PE, Geissmann F, Henri S, Malissen B, Osborne LC, Artis D, Mowat AM (2014) Constant replenishment from circulating monocytes maintains the macrophage pool in the intestine of adult mice. *Nat Immunol* 15: 929–937
- Battke F, Symons S, Nieselt K (2010) Mayday - integrative analytics for expression data. *BMC Bioinformatics* 11: 121
- Bertrand JY, Jalil A, Klaine M, Jung S, Cumano A, Godin I (2005) Three pathways to mature macrophages in the early mouse yolk sac. *Blood* 106: 3004–3011
- Bleriot C, Dupuis T, Jouvion G, Eberl G, Disson O, Lecuit M (2015) Liver-resident macrophage necroptosis orchestrates type 1 microbicidal inflammation and type-2-mediated tissue repair during bacterial infection. *Immunity* 42: 145–158
- Boring L, Gosling J, Chensue SW, Kunkel SL, Farese RV Jr, Broxmeyer HE, Charo IF (1997) Impaired monocyte migration and reduced type 1 (Th1) cytokine responses in C-C chemokine receptor 2 knockout mice. *J Clin Invest* 100: 2552–2561
- Cumano A, Godin I (2007) Ontogeny of the hematopoietic system. *Annu Rev Immunol* 25: 745–785
- Epelman S, Lavine KJ, Randolph GJ (2014) Origin and functions of tissue macrophages. *Immunity* 41: 21–35
- Erny D, Hrabec de Angelis AL, Jaitin D, Wieghofer P, Staszewski O, David E, Keren-Shaul H, Mhlakovich T, Jakobshagen K, Buch T, Schwierzeck V, Utermohlen O, Chun E, Garrett WS, McCoy KD, Diefenbach A, Staeheli P, Stecher B, Amit I, Prinz M (2015) Host microbiota constantly control maturation and function of microglia in the CNS. *Nat Neurosci* 18: 965–977
- van Furth R, Cohn ZA (1968) The origin and kinetics of mononuclear phagocytes. *J Exp Med*, 128: 415–435.
- Gautier EL, Shay T, Miller J, Greter M, Jakubczik C, Ivanov S, Helft J, Chow A, Elpek KG, Gordonov S, Mazloom AR, Ma'ayan A, Chua WJ, Hansen TH, Turley SJ, Merad M, Randolph GJ (2012) Gene-expression profiles and transcriptional regulatory pathways that underlie the identity and diversity of mouse tissue macrophages. *Nat Immunol*, 13: 1118–1128.
- Ginhoux F, Greter M, Leboeuf M, Nandi S, See P, Gokhan S, Mehler MF, Conway SJ, Ng LG, Stanley ER, Samokhvalov IM, Merad M (2010) Fate mapping analysis reveals that adult microglia derive from primitive macrophages. *Science* 330: 841–845
- Ginhoux F, Jung S (2014) Monocytes and macrophages: developmental pathways and tissue homeostasis. *Nat Rev Immunol* 14: 392–404
- Goldmann T, Wieghofer P, Muller PF, Wolf Y, Varol D, Yona S, Brendecke SM, Kierdorf K, Staszewski O, Datta M, Luedde T, Heikenwalder M, Jung S, Prinz M (2013) A new type of microglia gene targeting shows TAK1 to be pivotal in CNS autoimmune inflammation. *Nat Neurosci* 16: 1618–1626
- Gomez PE, Klapproth K, Schulz C, Busch K, Azzoni E, Crozet L, Garner H, Trouillet C, de Bruijn MF, Geissmann F, Rodewald HR (2015) Tissue-resident macrophages originate from yolk-sac-derived erythro-myeloid progenitors. *Nature* 518: 547–551
- Gosselin D, Link VM, Romanoski CE, Fonseca GJ, Eichenfield DZ, Spann NJ, Stender JD, Chun HB, Garner H, Geissmann F, Glass CK (2014) Environment drives selection and function of enhancers controlling tissue-specific macrophage identities. *Cell* 159: 1327–1340

- Hambleton S, Salem S, Bustamante J, Bigley V, Boisson-Dupuis S, Azevedo J, Fortin A, Haniffa M, Ceron-Gutierrez L, Bacon CM, Menon G, Trouillet C, McDonald D, Carey P, Ginhoux F, Alsina L, Zumwalt TJ, Kong XF, Kumararatne D, Butler K et al (2011) IRF8 mutations and human dendritic-cell immunodeficiency. *N Engl J Med* 365: 127–138
- Hashimoto D, Chow A, Noizat C, Teo P, Beasley MB, Leboeuf M, Becker CD, See P, Price J, Lucas D, Greter M, Mortha A, Boyer SW, Forsberg EC, Tanaka M, van Rooijen N, Garcia-Sastre A, Stanley ER, Ginhoux F, Frenette PS et al (2013) Tissue-resident macrophages self-maintain locally throughout adult life with minimal contribution from circulating monocytes. *Immunity* 38: 792–804
- Hochberg Y, Benjamini Y (1990) More powerful procedures for multiple significance testing. *Stat Med* 9: 811–818
- Hoeffel G, Wang Y, Greter M, See P, Teo P, Malleret B, Leboeuf M, Low D, Oller G, Almeida F, Choy SH, Grisotto M, Renia L, Conway SJ, Stanley ER, Chan JK, Ng LG, Samokhvalov IM, Merad M, Ginhoux F (2012) Adult Langerhans cells derive predominantly from embryonic fetal liver monocytes with a minor contribution of yolk sac-derived macrophages. *J Exp Med* 209: 1167–1181
- Hoeffel G, Chen J, Lavin Y, Low D, Almeida FF, See P, Beaudin AE, Lum J, Low I, Forsberg EC, Poidinger M, Zolezzi F, Larbi A, Ng LG, Chan JK, Greter M, Becher B, Samokhvalov IM, Merad M, Ginhoux F (2015) C-Myb(+) erythromyeloid progenitor-derived fetal monocytes give rise to adult tissue-resident macrophages. *Immunity* 42: 665–678
- Holtschke T, Lohler J, Kanno Y, Fehr T, Giese N, Rosenbauer F, Lou J, Knobloch KP, Gabriele L, Waring JF, Bachmann MF, Zinkernagel RM, Morse HC III, Ozato K, Horak I (1996) Immunodeficiency and chronic myelogenous leukemia-like syndrome in mice with a targeted mutation of the ICSBP gene. *Cell* 87: 307–317
- Huang LR, Wohlleb D, Reisinger F, Jenne CN, Cheng RL, Abdullah Z, Schildberg FA, Odenthal M, Dienes HP, Van RN, Schmitt E, Garbi N, Croft M, Kurts C, Kubas P, Protzer U, Heikenwalder M, Knolle PA (2013) Intrahepatic myeloid-cell aggregates enable local proliferation of CD8(+) T cells and successful immunotherapy against chronic viral liver infection. *Nat Immunol* 14: 574–583
- Jung S, Aliberti J, Graemmel P, Sunshine MJ, Kreutzberg GW, Sher A, Littman DR (2000) Analysis of fractalkine receptor CX3CR1 function by targeted deletion and green fluorescent protein reporter gene insertion. *Mol Cell Biol* 20: 4106–4114
- Kierdorf K, Erny D, Goldmann T, Sander V, Schulz C, Perdiguero EG, Wieghofer P, Heinrich A, Riemke P, Holscher C, Muller DN, Luckow B, Brocker T, Debowski K, Fritz G, Opendakker G, Diefenbach A, Biber K, Heikenwalder M, Geissmann F et al (2013) Microglia emerge from erythromyeloid precursors via Pu.1- and Irf8-dependent pathways. *Nat Neurosci* 16: 273–280
- Lavin Y, Winter D, Blecher-Gonen R, David E, Keren-Shaul H, Merad M, Jung S, Amit I (2014) Tissue-resident macrophage enhancer landscapes are shaped by the local microenvironment. *Cell* 159: 1312–1326
- Maere S, Heymans K, Kuiper M (2005) BiNGO: a Cytoscape plugin to assess overrepresentation of gene ontology categories in biological networks. *Bioinformatics* 21: 3448–3449
- McKercher SR, Torbett BE, Anderson KL, Henkel GW, Vestal DJ, Baribault H, Klemsz M, Feeney AJ, Wu GE, Paige CJ, Maki RA (1996) Targeted disruption of the PU.1 gene results in multiple hematopoietic abnormalities. *EMBO J* 15: 5647–5658
- Merico D, Isserlin R, Stueker O, Emili A, Bader GD (2010) Enrichment map: a network-based method for gene-set enrichment visualization and interpretation. *PLoS One* 5: e13984
- Mildner A, Schmidt H, Nitsche M, Merkler D, Hanisch UK, Mack M, Heikenwalder M, Bruck W, Priller J, Prinz M (2007) Microglia in the adult brain arise from Ly-6C(hi)CCR2(+) monocytes only under defined host conditions. *Nat Neurosci* 10: 1544–1553
- Molawi K, Wolf Y, Kandalla PK, Favret J, Hagemeyer N, Frenzel K, Pinto AR, Klapproth K, Henri S, Malissen B, Rodewald HR, Rosenthal NA, Bajenoff M, Prinz M, Jung S, Sieweke MH (2014) Progressive replacement of embryo-derived cardiac macrophages with age. *J Exp Med* 211: 2151–2158
- Newman AM, Liu CL, Green MR, Gentles AJ, Feng W, Xu Y, Hoang CD, Diehn M, Alizadeh AA (2015) Robust enumeration of cell subsets from tissue expression profiles. *Nat Methods* 12: 453–457
- Oesper L, Merico D, Isserlin R, Bader GD (2011) WordCloud: a Cytoscape plugin to create a visual semantic summary of networks. *Source Code Biol Med* 6: 7
- Prinz M, Priller J (2014) Microglia and brain macrophages in the molecular age: from origin to neuropsychiatric disease. *Nat Rev Neurosci* 15: 300–312
- Rosenbauer F, Tenen DG (2007) Transcription factors in myeloid development: balancing differentiation with transformation. *Nat Rev Immunol* 7: 105–117
- Schonheit J, Kuhl C, Gebhardt ML, Klett FF, Riemke P, Scheller M, Huang G, Naumann R, Leutz A, Stocking C, Priller J, Andrade-Navarro MA, Rosenbauer F (2013) PU.1 level-directed chromatin structure remodeling at the irf8 gene drives dendritic cell commitment. *Cell Rep* 3: 1617–1628
- Schulz C, Gomez PE, Chorro L, Szabo-Rogers H, Cagnard N, Kierdorf K, Prinz M, Wu B, Jacobsen SE, Pollard JW, Frampton J, Liu KJ, Geissmann F (2012) A lineage of myeloid cells independent of Myb and hematopoietic stem cells. *Science* 336: 86–90
- Scott CL, Zheng F, De BP, Martens L, Saey Y, De PS, Lippens S, Abels C, Schoonooghe S, Raes G, Devoogdt N, Lambrecht BN, Beschin A, Williams M (2016) Bone marrow-derived monocytes give rise to self-renewing and fully differentiated Kupffer cells. *Nat Commun* 7: 10321
- Sheng J, Ruedl C, Karjalainen K (2015) Most tissue-resident macrophages except microglia are derived from fetal hematopoietic stem cells. *Immunity* 43: 382–393
- Shiau CE, Kaufman Z, Meireles AM, Talbot WS (2015) Differential requirement for irf8 in formation of embryonic and adult macrophages in zebrafish. *PLoS One* 10: e0117513
- Sieweke MH, Allen JE (2013) Beyond stem cells: self-renewal of differentiated macrophages. *Science* 342: 1242974
- Tamura T, Ozato K (2002) ICSBP/IRF-8: its regulatory roles in the development of myeloid cells. *J Interferon Cytokine Res* 22: 145–152
- Tamura T, Yanai H, Savitsky D, Taniguchi T (2008) The IRF family transcription factors in immunity and oncogenesis. *Annu Rev Immunol* 26: 535–584
- Theocharidis A, van Dongen S, Enright AJ, Freeman TC (2009) Network visualization and analysis of gene expression data using BioLayout Express(3D). *Nat Protoc*, 4: 1535–1550.
- Wilson K, Grenfell BT (1997) Generalized linear modelling for parasitologists. *Parasitol Today* 13: 33–38
- Yona S, Kim KW, Wolf Y, Mildner A, Varol D, Breker M, Strauss-Ayali D, Viukov S, Williams M, Misharin A, Hume DA, Perlman H, Malissen B, Zelzer E, Jung S (2013) Fate mapping reveals origins and dynamics of monocytes and tissue macrophages under homeostasis. *Immunity* 38: 79–91